ARTICLES

Interaction of a Polycation with Small Oppositely Charged Dendrimers

H. Zhang[†] and P. L. Dubin*

Department of Chemistry, Indiana-Purdue University, Indianapolis, Indiana 46202-3274

J. Ray and G. S. Manning

Department of Chemistry, Rutgers University, Piscataway, New Jersey 08854-8087

C. N. Moorefield and G. R. Newkome

Department of Chemistry, University of South Florida, Tampa, Florida 33620-5250

Received: August 21, 1998; In Final Form: January 13, 1999

Complex formation between small carboxyl-terminated dendritic polymers and oppositely charged poly(dimethyldiallylammonium chloride) was monitored by turbidimetry, dynamic light scattering, viscometry and potentiometric titration. All techniques reveal a discontinuity at a well-defined pH, corresponding to the point of incipient complex formation. Conversion of this critical pH to a surface charge density σ_{crit} leads to the observation that σ_{crit}, to a first approximation, varies linearly with the Debye−Hückel parameter κ and that binding occurs more easily (i.e., at lower σ_{crit}) for the larger dendrimer. A model is presented in which the distortion of the polyelectrolyte backbone in the complex is described in terms of the elastic resistance to bending around the contour of the spherical macroion, acting in opposition to attractive Coulombic forces. The elastic resistance is treated as a Hookean effect obtained from the measured persistence length. This simple theory produces the principal features of the experimental system.

Introduction

The interaction of polyelectrolytes with oppositely charged colloids is important in the context of several technological problems and is also relevant to some biological phenomena. Polyelectrolytes are used to stabilize or destabilize colloidal systems in, for example, paper-making, sludge dewatering, producing pigment coatings, and water purification; typically the particles carry negative charges and the polyelectrolytes are cationic. In the biological realm, the interaction of DNA with proteins and with chromatin is known to have a strong electrostatic component and to involve positively charged regions arising from basic amino acid residues. Systems that are partially natural have also been of interest: the complexation of synthetic polyelectrolytes with globular proteins has been examined from the point of view of enzyme stabilization[1], microencapsulation,[2] and protein purification.[3]

Such phenomena have attracted theoretical consideration. In one approach, polyelectrolyte adsorption is considered as a modification of the adsorption of neutral polymers, in which the entropy of adsorbed and free chains plays a major role. The problem was first treated by Wiegel[4] and, subsequently, Muthukumar.[5] Evers and co-workers modified the self-consistent mean-field theory developed for neutral polymer adsorption to the case of weak polyelectrolyte adsorption.[6] Odijk[7] took a very different approach to the problem, largely guided by some experimental findings.[8] While refs 4−7 all treat the adsorbing surface as a plane, subsequent modifications to allow for colloid surface curvature produced only modest changes in the theoretical results.[9] Despite the remarkable variation in the approaches pursued in the aforementioned treatments, all of them lead to the prediction of phase-transition-like behavior, i.e., the appearance of a bound polymer state when the charge density of the surface attains some critical value. In general, the result may be expressed as

$$\sigma_{crit} \sim \xi^{-1}\kappa^{a} \tag{1}$$

where ξ is the linear charge density of the polyion (usually given as the charge per repeat unit q, but perhaps more clearly presented as Manning's reduced charge density), and κ is the Debye−Hückel parameter. Typically, the temperature appears in eq 1, but since it evolves from a Boltzmann term, and thus with neglect of the manifold effects of temperature on, for example, ion solvation, water structure, and especially the entropy of small ions, the temperature provides little guide to experiment. Thus, the only difference in the conclusions of refs 4−7 is the exponent a, which appears as unity in refs 6 and 7, as three in ref 4, and as $^{11}/_{5}$ in ref 5 (with some dependence on ionic strength).

A dramatically different approach has been taken toward the binding of proteins to DNA by Manning[10] and by Record.[11] In this case the protein is considered as essentially a large counterion, and the polymer chain entropy is, with good reason,

[†] Current address: SLTP Co. Ltd., 588 Jiu Xing Rd., Shanghai 20614, PRC.

10.1021/jp983436y CCC: $18.00
Published on Web 03/13/1999

neglected. In that case, no phase-transition type behavior is predicted, and the theoretical result is instead a semilogarithmic dependence of the binding constant on the ionic strength, the binding decreasing with added salt to the z_2/z_1 power, where z_2 and z_1 are valences of ligand and salt. z_2 signifies the charge on the area of the protein that binds to DNA so that the interaction is visualized as having geometric specificity.

The predictions of refs 4−7 seem to be supported by work involving synthetic polyelectrolytes and either oppositely charged micelles, or proteins. To summarize these findings,[12] a wide variety of techniques, including turbidimetry, total intensity measurements, dynamic light scattering, potentiometric titration, electrophoretic light scattering, and Cryo-TEM all seem to point to a rather well-defined colloid surface charge density σ_{crit} corresponding to incipient complex formation. In general, a change of only one or two percent in σ suffices to produce dramatic changes in the experimental measurables corresponding to the above-mentioned techniques. The ionic strength dependence of σ_{crit} and the effect of ξ both seem to point toward the validity of eq 1 with $a = 1$. Despite the rather good fit to $\sigma_{crit}\xi \sim \kappa$ for polyelectrolyte-colloid systems with colloid particles as small as ca. 5 nm (e.g., bovine serum albumin[13] or spherical micelles of dimethyldodecylamine-*N*-oxide[14]), the agreement between experiment and theories based on planar surfaces must be viewed with some skepticism. For colloids of high surface curvature, the number of polymer segments involved in the interaction must be small, and polymer configurational chain entropy must play a diminished role. Indeed, models based on counterion condensation become more attractive for such small particles. It is therefore of interest to examine the interaction between polyelectrolytes and particles in the size regime intermediate between the ranges normally assigned to counterions and colloids respectively, i.e., on the order of a few nanometers. From this point of view, theoretical treatments developed from the perspective of counterion binding assume a more attractive position. On the other hand, these intermediate-sized particles are too large to be characterized simply by their total charge, or "valence", since their radii are comparable to the Debye screening length of the solution.

Recently, Wallin and Linse[15] published the results of simulations of the binding of a flexible chain to an oppositely charged spherical micelle. Their "snapshots" show that increased chain stiffness results in decreased binding and also yield insight into the effects of micelle size. While their model is highly detailed, they do not emphasize the dependence of binding on ionic strength nor do they indicate a critical charge density, choosing rather to compare their results to reported experimental values of the "critical aggregation concentration", the surfactant concentration at which polyelectrolyte−surfactant complexes appear. In such experimental systems, one confronts the likelihood that the complexes so formed contain surfactant clusters that are not identical to the micelles per se. This points to the need to compare simulations and theory for polyelectrolyte−sphere systems with experimental studies done on intact colloidal particles.

Carboxyl-terminated dendritic polymers are appropriate models for small, highly charged colloids. Within the realm of achievable synthesis (precluding branch defects), the range of MWs is 10^3-10^5, corresponding to diameters of 1−10 nm.[16] Terminal groups become more congested with increasing generation number *G*, with the area per terminus decreasing from about one to 0.3 nm^2. These correspond to very large surface charge densities for the higher generations, and these surface charge densities may be easily varied by pH adjustment. Thus, dendrimers are particles of well-defined shape and size with uniform and controllable surface charge densities. The smaller dendrimers ($G < 3$) are thought to be oblate as opposed to strictly spherical and may also reveal expansion in response to charge repulsion among carboxylic acid groups, e.g., upon pH increase at low ionic strength;[17] nevertheless, there are clear advantages in their use as model particles, relative to other colloids. In carboxylated or sulfonated latex microspheres, ionic groups may be located at interior positions, and this effect may be manifested in time-dependence of titration behavior. Silica microspheres do not exhibit this complication but tend to aggregate at low pH and moderate ionic strength. With micelles, both of these problems may be avoided, but then the dynamic nature of colloidal structure must be confronted. And proteins, of course, are characterized by highly irregular geometry and surface charge heterogeneity.

We previously reported[18,19] on complex formation between the strong polycation, poly(dimethyldiallylammonium chloride) (PDADMAC) and carboxyl-terminated PAMAM[16] dendrimers (CT-PAMAM). By turbidimetry and by dynamic light scattering, we observed the abrupt formation of complexes at a well-defined pH (pH_{crit}) which increased with ionic strength. The onset of complex formation could also be followed by measuring the deviation between pH titration curves obtained with CT-PAMAM in the presence and absence of polycation. pH_{crit} was found to decrease with increasing generation number, as expected based on the increase in carboxyl surface density; for G1 at moderate ionic strength, no complexation could be observed. However, although we could measure pH_{crit}, we could not convert these values to σ_{crit}: this conversion requires a knowledge of the dependence of the degree of dissociation of the surface carboxyl groups (α) as a function of pH (i.e. the titration curve) but attempts to obtain this dependence showed that the titration curve was complicated by the presence of interior tertiary amines. The presence of these titratable amines was also manifested in the observable precipitation of a polyanion, sodium poly(styrenesulfonate), by CT-PAMAM at low pH.

For the foregoing reasons, studies have been initiated with carboxyl-terminated cascade polymers[20,21] which have no interior titratable groups. The "ideal" electrostatic behavior of these dendrimers is suggested by analysis of their titration curves,[21] from which one may calculate the relationship between surface potential and surface charge density. For the low generation dendrimers, this dependence is exactly congruent with solution of the nonlinearized P−B equation; for higher G, the deviations that occur can be understood in terms of Na^+ binding. CT-CPs thus appear to be useful as models to test electrostatic theories and have been used by us to evaluate theoretical predictions for the permeation of charged spheres into like-charge cavities.[22] In the current study, we focus on the interaction of two small CT-CPs, namely G1 and G3, in the presence of PDADMAC, using a polymer with a more narrow MWD than the sample employed in previous studies.[17,18] There are two objectives in the present work: the first is to determine whether this system exhibits "phase boundary" behavior consistent with eq 1; the techniques employed are turbidimetry, quasielastic light scattering, potentiometric titration and dilute solution viscometry. The second is to establish whether a simple and intuitively clear model based on classical concepts from ionic solution theory can account for the essential features of the binding phenomena.

TABLE 1: Characteristics of Carboxyl-Terminated Dendrimers

generation	theoretical number of terminal COOH	theoretical MW	R_s (nm)
1	12	1341	1.2[a]
3	108	12345	2.0[b]

[a] By NMR (diffusion coefficient was obtained by pulsed field gradient NMR, and R_s was calculated with the Stokes−Einstein equation) in water.[20] [b] By QELS in 0.10 M NaCl.

Experimental Section

Materials and Methods. *Materials.* Synthesis and purification of polydiallydimethylammonium chloride (PDADMAC) was carried out at in the laboratory of Prof. W. Jaeger at the Fraunhofer Institut (Teltow, Germany). The polymer was ultrafiltered, freeze-dried and characterized by membrane osmometry ($M_n = 1.5 \times 10^5$). Carboxylic acid terminated cascade polymers (Z-Cascade:methane[4]:(3-oxo-6-oxa-2-azaheptylidyne):(3-oxo-2-azaheptylidyne):propanoic acids) (hereafter referred to as dendrimers) were prepared by procedures described elsewhere.[20] Table 1 shows the characteristics of cascade polymers generations 1 and 3 (G1 and G3).

Standard NaOH (0.100 N) and HCl (0.100 N) solutions and analytical grade NaCl were from Fisher Scientific (Pittsburgh, PA). Milli-Q water was used throughout this study.

Titrations. "Type I" titrations were performed, at fixed ionic strength, by adjusting the pH of a solution of PDADMAC + dendrimer. In "type II" titrations, dendrimer was added to a solution at selected initial PDADMAC concentration and pH. "Type III" titrations involved addition of PDADMAC to a solution at some initial dendrimer concentration and pH. A 2 mL Gilmont microburet readable to 0.002 mL was used. All titrations were performed under moderate stirring.

Turbidimetry. Turbidity recorded as 100 − T% at 420 nm was measured at 24 ± 1 °C using a Brinkman PC800 probe colorimeter equipped with a 1 cm path length fiber optics probe and adjusted to read 100% transmittance with Milli-Q water. All solutions were filtered through 0.45 μm Whatman filters before turbidimetric titration. All measured values from turbidimetric type I titrations were corrected by subtracting the turbidity of a polymer-free blank.

Quasi-Elastic Light Scattering Measurements. Samples were introduced via 0.1 μm Anotec filters into the 7 μL cell of a DynaPro 801 (Protein Solutions, Inc., Charlottesville, VA). This instrument employs a 30 mW solid-state 780-nm laser and an avalanche photodiode detector. Total scattering intensities (90°) and apparent Stokes radii (via the method of cumulants) were determined at 23 ± 1.5 °C for types I, II, and III titrations.

Viscosity Measurements. Viscometric type I and type II titrations were conducted using a Schott Geräte AVS 3000 device equipped with a Ubbelohde dilution viscometer at 25 ± 0.1 °C. All solutions were filtered through 0.45 μm Whatman filters. The efflux time error was ± 0.01 s. The reported reduced viscosity is defined here as

$$\eta_{red} = \frac{\left(\frac{t_s}{t_o} - 1\right)}{C_p} \tag{2}$$

where t_s and t_o are the efflux time of a sample solution and a solvent, respectively, and C_p is polymer concentration.

Potentiometric Titrations. pH titrations were conducted using a Beckman Φ34 pH meter equipped with a Beckman No. 39848 combination electrode under nitrogen atmosphere at 24 ± 1 °C. The error of the buffer solutions for pH 4.00 and 7.00 is ± 0.01 pH, and the error for pH 10.00 buffer solution is ± 0.02 pH. The instrumental pH drift was less than 0.02 pH/hr.

Calculations. The relationship between the apparent dissociation constant K_a and the degree of ionization α of the carboxylic groups of a polyacid is described as

$$pKa = pH + \log\frac{1-\alpha}{\alpha} \tag{3}$$

where α is defined as

$$a = \frac{[COO^-]}{[COOH] + [COO^-]} \tag{4}$$

The pH of a polyacid solution can be generally described by[23]

$$pH = pK_o - \log\frac{1-\alpha}{\alpha} + \frac{0.434}{RT}\left(\frac{\partial G_{el}}{\partial \alpha}\right) \tag{5}$$

where pK_o, the intrinsic dissociation constant, is obtained by extrapolating pK_a to $\alpha = 0$ and is the electrostatic Gibbs free energy change per unit degree of $\partial G_{el}/\partial\alpha$ dissociation, R is the molar gas constant, and T is the temperature.

Combination of eqs 3 and 5 leads to

$$pK_a - pK_o = \frac{0.434}{RT}\left(\frac{\partial G_{el}}{\partial \alpha}\right) \tag{6}$$

The right-hand side of eq 6 may be related to the surface potential by

$$\frac{\partial G_{el}}{\partial \alpha} = -eN_a\psi_o \tag{7}$$

where e is the elementary electric charge (C) and N_a is Avogadro's number.

Combining eqs 6 and 7 leads to eq 8:

$$\psi_o = -(pK_a - pK_o)\frac{kT}{0.434e} \tag{8}$$

where k is Boltzmann constant. Thus, the surface potential, ψ_o, at the site where H^+ originates, can be obtained experimentally via eq 8.

For uniformly charged spheres, the potential (ψ) at a distance r from the center, in a symmetrical 1−1 electrolyte, can be calculated via the Poisson−Boltzmann (P−B) equation,

$$\frac{\partial}{r^2\partial r}\left(r^2\frac{\partial \psi}{\partial r}\right) = \frac{8\pi en}{D}\sinh\frac{e\psi(r)}{kT} \tag{9}$$

where n is the electrolyte concentration and D the dielectric constant, here set at 78.5. Numerical solutions of the nonlinear P−B equation were done using Mathematica 2.2, with the boundary conditions $[\partial\psi/\partial r]_{r=a}$ $(= -4\pi\sigma/\epsilon)$ and $\psi_{r=\infty} = 0$. For G3, hydrodynamic radii, measured by QELS as a function of pH and I, were used as the distance from the center of the dendrimer to the dissociation position. For G1, weak scattering prohibited definitive results; therefore, a radius of 1.2 nm, obtained by NMR,[17] was used. After obtaining a numerical value of $[\partial\psi/\partial r]_{r=a}$ at each α_c and corresponding ψ_0, σ_c^{ϕ} was obtained as $-\epsilon[\partial\psi/\partial r]_{r=a}/4\pi$.

The formal or "geometric" surface charge density can be calculated from the number of ionized carboxylate groups per

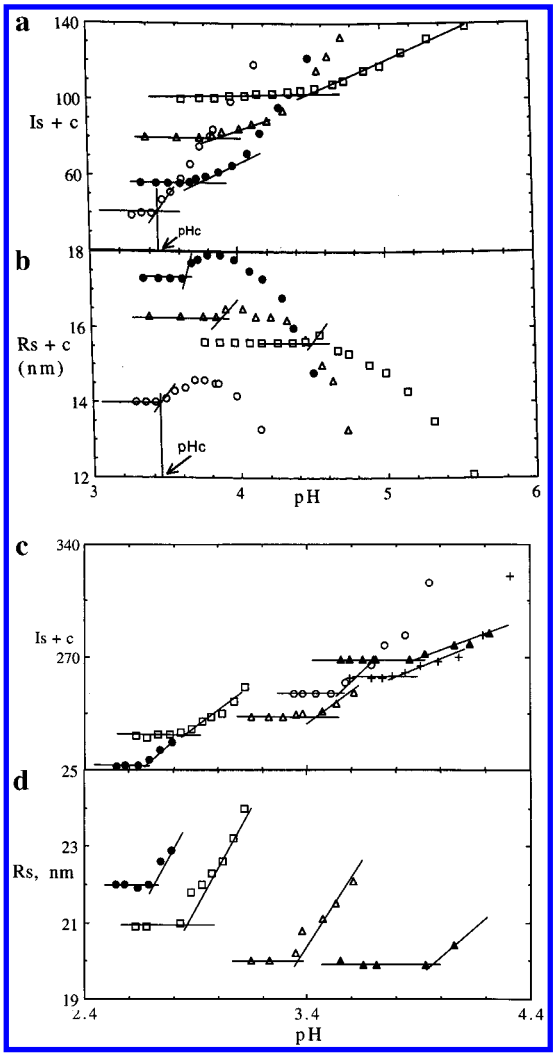

Figure 1. (a) and (b): Effect of pH on (a) scattering intensity and (b) apparent Stokes radius, for G1 (0.3 g/L) + PDADMAC (0.5 g/L) at ionic strengths: (○) 0.01, (●), 0.05, (△) 0.10, (□) 0.20. (c) and (d): Effect of pH on (c) scattering intensity and (d) apparent Stokes radius, for G3 (0.3 g/L) + PDADMAC (0.5 g/L) at ionic strengths: (●) 0.05, (□) 0.10, (△) 0.20, (▲) 0.50.

unit surface area:

$$\sigma^{g} = \frac{N\alpha e}{4\pi a^{2}} \qquad (10)$$

where N is the total number of carboxyl groups and a is the radius of the cascade polymer.

Results

Critical Conditions for Complex Formation. Figure 1a shows the dependence of scattered light intensity I_s on pH for G1 + PDADMAC. The pH at which the intensity departs from a constant value, pH_c, corresponds to the onset of complex formation. With further increase in pH, the intensity increases, with the solutions remaining visibly clear until a second critical pH (pH_ϕ, not shown here), is attained, at which point phase separation occurs. Figure 1b shows the pH dependence of the apparent Stokes radius R_s^{app} which also displays a change in slope at the same pH_c . For $pH > pH_c$, the behavior of R_s^{app} is somewhat complex, particularly for $I \leq 0.1$. The dependence of R_s^{app} on pH seen for G3 + PDADMAC shown in Figures 1c and d is more straightforward.

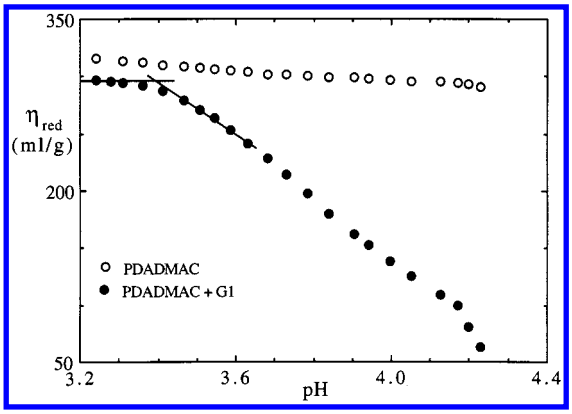

Figure 2. Reduced viscosity of (○) PDADMAC (0.5 g/L) alone (○) and with ● G1 (0.3 g/L) + PDADMAC (0.5 g/L) in 0.10 M NaCl at 25 °C. Break point corresponds to "pH_c".

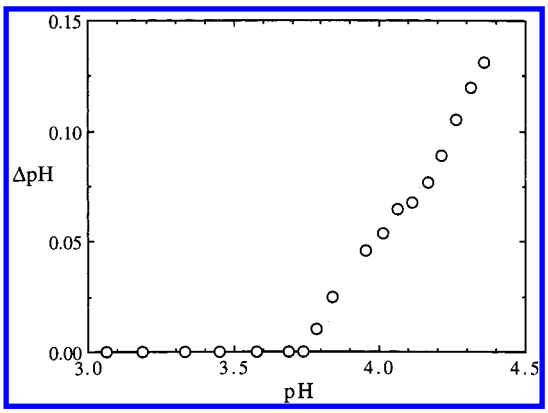

Figure 3. Effect of the presence of PDADMAC (0.5 g/L) on the pH titration curve of G1 (0.3 g/L) in 0.10 M NaCl, presented as pH difference between titration curves, with and without polymer, vs pH. Nonzero values for ΔpH correspond to complex formation.

To verify the determination of pH_c for G1+PDADMAC, two other techniques were employed. The reduced viscosity of PDADMAC, with 0.3 g/L G1+0.01M NaCl defined as the solvent, was measured as a function of pH with the results shown in Figure 2. The contribution of G1 to the measured viscosity was virtually negligible. The viscosity departs from a constant value at pH = 3.4 which agrees very well with pH_c from QELS for this system. As a second technique, potentiometric titration was carried out for G1 in 0.1 M NaCl, with and without PDADMAC. Since the only titratable groups present are the dendrimer carboxylic acids, differences between these two titration curves can be attributed to pK shifts induced by complex formation. In Figure 3 we plot the diminution in pH that would occur if PDADMAC were added to a solution of dendrimer at some initial pH. In the absence of complex formation, ΔpH = 0. The onset of complexation as measured by a decrease in the effective pK_a of the dendrimer is observed at pH = 3.75, in good agreement with $pH_c = 3.80$, from Figure 1a.

According to eq 1, the critical surface charge density at constant ξ should vary with κ. Values of pH_c determined as shown in Figure 1 were converted to α_c using the pH titration curves at the appropriate ionic strengths. Equation 10 was then employed to obtain the geometric surface charge density. The open symbols in Figure 4 show the dependence of σ^g_c on $I^{1/2}$ for G1 and G3. While the data for G1 conform to a linear dependence of σ on κ, within experimental error, the data for G3 do not. In a separate study[21] we found that the dependence of ψ_o on σ^g followed the P−B equation for G1, but not for

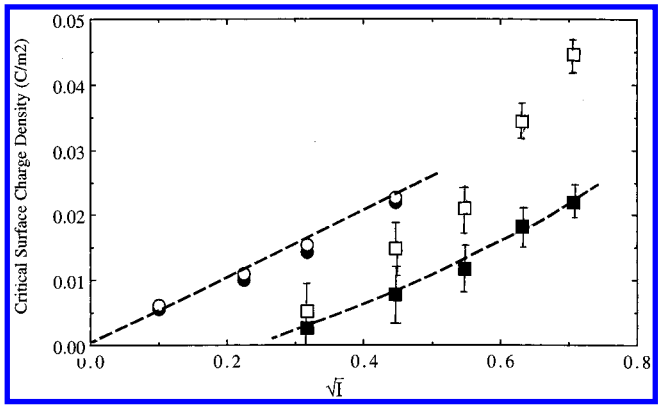

Figure 4. Ionic strength dependence of critical surface charge density for complexation. G1: (○) (σ, geom), (●) (σ, pot). G3: (□), (σ, geom), (■) (σ, pot).

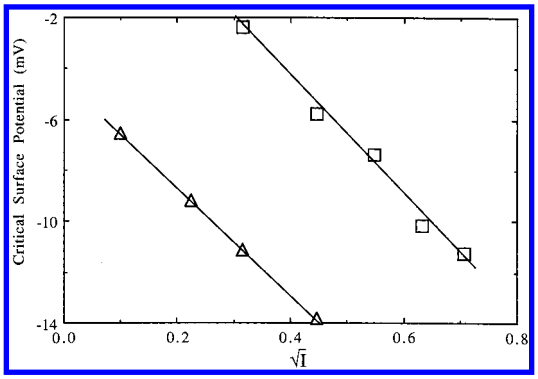

Figure 5. Ionic strength dependence of critical surface potential for complexation: (△) G1; (□) G3.

higher generations. The depression of ψ_o for G3 could be understood as a consequence of counterion (Na^+) binding.

Since σ^g may overestimate the effective surface charge density of G3, we calculated σ^{ϕ}_c using eq 9. As shown in Figure 4, the dependence of σ^{ϕ}_c on $I^{1/2}$ for G1 conforms, within experimental error, to eq 1 with $\lambda = 1$, while the results for G3 are nearly linear but display some perceptible curvature at higher ionic strength. As noted above, we believe that the divergence between σ^{ϕ}_c and σ^g_c for G3 corresponds to counterion condensation. As expected, σ^{ϕ}_c and σ^g_c are identical for G1. Finally, we note that the slopes for G1 and G3 are nearly the same, as predicted by eq 1, since $\partial\sigma/\partial\kappa$ should depend only on ξ.

The ionic strength dependence of the critical surface potential, shown in Figure 5, may be recognized as a phase boundary, in which the region intermediate between the two curves shows conditions under which G3 complexes but G1 does not. The diminished stability of the G1 complex, compared to G3 at the same surface potential, may be understood as a consequence of the high surface curvature of the former. The binding energy must depend on the number of polymer segments located near the surface of the dendrimer. If the number of "contacts" between polycation and cascade polymer were the same for complexes with G1 and G3, the configuration of the bound polymer would be more highly constrained for the more highly curved G1, with a loss of chain entropy. Consequently, the binding of G1 is less favorable so that a higher surface potential is required. In this description, the polycation is rather simplistically viewed as infinitely flexible. An alternate explanation can be formulated in terms of the elastic resistance of chains with finite persistence length, and this representation forms the basis of the theoretical approach that follows.

Theoretical Section

Model and Method. In the theoretical portion of this paper, we attempt to explain why binding is observed to occur only above a threshold surface charge density on the macroion (dendrimer), which increases in proportion to the square root of ionic strength, and why the critical charge density varies with the radius of the macroion. The length of a binding site on the polymer is comparable to a persistence length, and the relative sizes of polymer binding segment and macroion radius are such that considerable bending of the former must occur upon binding to the spherical macroion. We suggest that the attractive electrostatic forces responsible for binding are resisted by the bending stress stored in the polymer as it deforms around the macroion in order to bring its charged sites into proximity with the charged sites on the macroion. A decreased electrostatic attractive energy would then be obtained only at the expense of an increased elastic energy of bending, and the attendant competition between these two energy sources may constitute the principal factor determining binding.

This simple picture has been previously developed in connection with the binding of DNA to an octamer of basic histone proteins[24,25] The model is able to explain the observation of abrupt transitions of nucleosome structure as a consequence of the elastic instability of the wrapped DNA. Movement of the DNA onto and off the histone octamer does not occur progressively but in abrupt jumps among positions near and far from the octamer surface. The persistence length of DNA is very large, as is the correlated Hooke's law constant for DNA bending, and the large amount of elastic energy stored along a stiff and relatively long piece of bent DNA can result in abrupt conformational changes. We do not observe this behavior in the more flexible chains analyzed here. As we will show, however, the elastic bending energy of flexible chains complexing to small macroions is sufficient to generate behavior that is not too different from the characteristics of the nucleosome complex and, in particular, is sufficient to explain a threshold charge density for binding with the experimentally observed ionic strength and size dependence.

As noted above, the images presented from the simulations of Wallin and Linse[15] show that increased chain stiffness results in decreased binding, and some of their pictures can be interpreted as supporting the basic idea used here. However, we have approached the problem more from the point of view of classical theory. From this standpoint, the question we ask, and partially answer, is whether a simple Hooke's law elastic description of bending can be useful when combined with classical concepts from ionic solution theory.

In our simplified picture of the binding of a polymer to an oppositely charged macroion, the polymer wraps onto the surface of the spherical macroion in a plane. The macroion is then represented by an impenetrable circle. The charged groups on the spherical surface are taken as discrete points with fractional charges q_i spaced uniformly along the circle, the spacing fixed at a convenient value. The fractional charge is adjusted to the value that induces binding of the polymer. A correspondence between this spacing and charge and the surface charge density on the spherical macroion is set up (with neglect of macroion curvature). The polymer is represented by a linear array of univalent point charges with uniform spacing 6.5 Å (the contour length per residue is 6.5 Å for PDADMAC, and there is one unit charge per residue). To consider local steric constraints on the polymer, we have introduced a distance of closest approach between a positive charge on the polymer and a negative charge on the macroion surface.

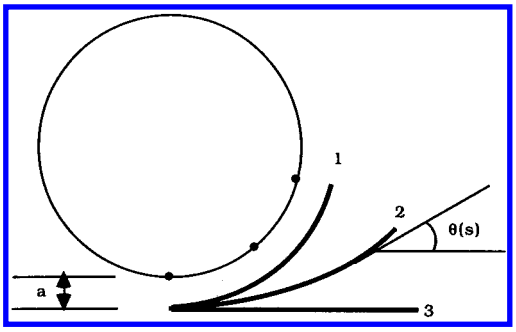

Figure 6. Pictorial representation of the model binding system, with three representative paths of the polymer binding segment.

The model shown in Figure 6 depicts the movement on and off the particle surface of the set of cooperatively bound residues that we refer to as the polymer segment. Three possible trajectories of the segment are shown. All of them start at a common initial point which remains attached to the particle. Curve 1 represents the trajectory of the fully associated polymer. Curve 3 is the same segment, fully dissociated. Curve 2 shows an intermediate trajectory between complete binding and complete dissociation. It is assumed that configurations such as curves 2 and 3 are so weakly associated with the macroion that immediate dissociation would occur. Only the configuration of curve 1 is sufficiently stable to be detected by the current measurements.

The total potential energy of the polymer segment is assumed to have two contributions. The first takes into account the locally elastic character of the polymer, which forces polymer bending to occur only at the expense of the storage of a certain amount of bending energy E_{bend}. E_{bend} is taken from the classical elastic theory of a thin isotropic rod. The second contribution, $E_{\text{macroion-polymer}}$, gives the amount of energy available from the attractive macroion−polymer forces. The charges on the polymer interact with the opposite charges on the macroion with a potential represented by a Debye−Hückel pairwise interaction. The total energy can then be written as

$$E = E_{\text{bend}} + E_{\text{macroion-polymer}} \tag{11}$$

where the bending energy term is positive, and the interaction term is negative.

For E_{bend}, we use Hooke's law,

$$E_{\text{bend}} = \frac{1}{2} b \int_0^L 1/\rho^2 \, \mathrm{ds} \tag{12}$$

where b is the elastic constant for bending, s is the contour length along the polymer segment measured from the point of anchor in Figure 6, $1/\rho$ is the curvature of the segment at position s, and L is the length of the binding segment. The numerical value of b is obtained by the standard formula

$$b = kT\lambda \tag{13}$$

where kT is the product of Boltzmann's constant and Kelvin temperature, and λ is the persistence length of the polymer.

The attractive electrostatic energy of interaction between the polymer and the dendrimer is obtained by adding Debye−Hückel screened Coulomb potentials between all pairs of positive and negative charges with a distance of closest approach a. Thus,

$$E_{\text{macroion-polymer}} = -\sum_i^N \sum_j^P \frac{q_i q_j \exp[-\kappa(r_{ij} - a)]}{D r_{ij}(1 + \kappa a)} \tag{14}$$

where r_{ij} is the distance between the ith charge on the macroion and the jth charge on the polymer, N is the number of charges on the macroion (i.e., on the circle in Figure 6), P is the number of charges on the polymer binding segment, q_i and q_j are the values of the macroion and polymer charges, respectively (q_i is fractional as explained above, while q_j is the unit positive charge), D is the dielectric constant, and κ is the Debye screening parameter, given at room temperature by

$$\kappa = 0.329\sqrt{c} \ (\text{Å}^{-1}) \tag{15}$$

where c is the molarity of 1:1 salt.

The energies in eqs 12 and 14 are computed along the trajectory of the polymer segment. The trajectories, all of total contour length L, the length of the polymer binding segment, are represented by the first two terms of a series expansion in powers of the length variable s

$$\theta(s) = x_1\left(\frac{s}{L}\right) + x_2\left(\frac{s}{L}\right)^2 \tag{16}$$

where $\theta(s)$ is the angle of inclination toward the horizontal made by the tangent to the polymer path drawn at length s along the path (Figure 6). If the coefficient x_2 equals zero, the trajectory is the arc of a circle with constant curvature x_1/L. Assigning negative values to x_2 allows the polymer path to straighten from a circular arc. Our previous experience with this method suggests that it is not necessary to search for a minimum-energy path among a field wider than indicated in eq 16.[24,25]

The (x, y) coordinates of the charged groups along the polymer curve are obtained from the following expressions

$$x(s) = \int_0^s \cos\theta \, \mathrm{ds}, \quad y(s) = \int_0^s \sin\theta \, \mathrm{ds} \tag{17}$$

The starting point of the polymer segment is set at the origin: $x(0) = y(0) = 0$.

The total energy of the polymer segment, that is, the sum of the energies given by eqs 12 and 14, is evaluated numerically for given values of x_1 and x_2 at a particular ionic strength, i.e., value of κ. We get the stable equilibrium path of the polymer by minimizing the total energy over various paths (various values of x_1 and x_2).

The total energy $E_{\text{bend}} + E_{\text{macroion-polymer}}$ of a specific polymer trajectory is a fixed quantity for a given ionic strength. So minimization of the total energy over polymer trajectories results in a single minimum-energy path. If, in calculating the macroion charges q_i in eq 14, the critical dendrimer surface charge density is set to that found experimentally to induce binding, we find that the resulting minimum-energy path does not represent a bound segment, but is partially unwrapped from the particle surface, like curve 2 in Figure 6. The meaning is that the forces of attraction between macroion and polymer in the form of eq 14 are, in our model, insufficiently strong to overcome the intrinsic resistance to bending the polymer onto the dendrimer, in conflict with the experimental result that the polymer binds at the surface charge density used in the calculations. The Debye−Hückel potential in eq 14 was therefore modified by multiplying it by an adjustable factor M, a catch-all parameter reflecting modeling inaccuracies. The interaction energy is now written as

$$E_{\text{macroion-polymer}} = -M\sum_i^N \sum_j^P \frac{q_i q_j \exp[-\kappa(r_{ij} - a)]}{D r_{ij}(1 + \kappa a)} \tag{18}$$

where q_i, as before, is the value of the macroion charges found

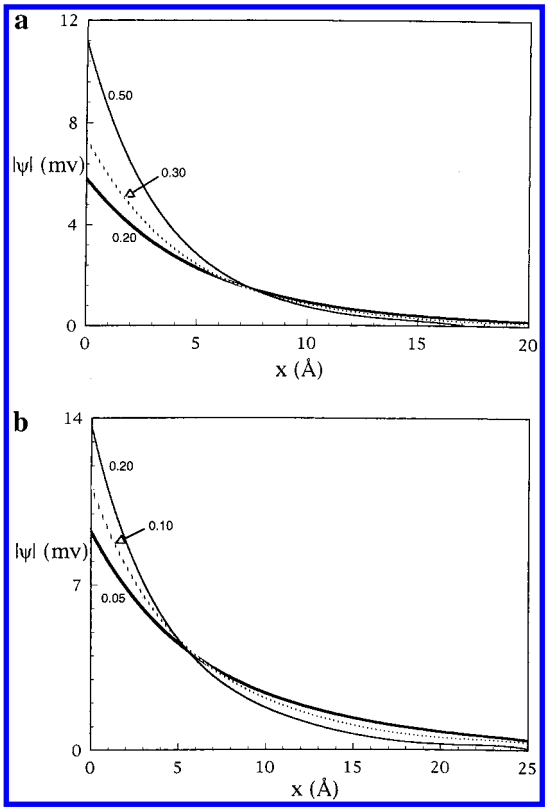

Figure 7. Screened potential vs distance, corresponding to critical binding conditions at ionic strengths shown, for (a) G1 and (b) G2.

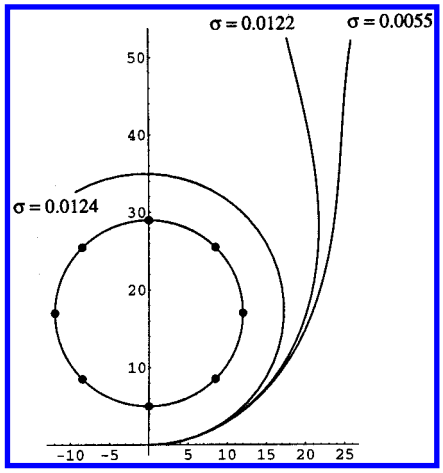

Figure 8. Minimum-energy trajectories of the polymer binding segment for several values of the macroion surface charge density σ (C m^{-2}). Each trajectory shown is labeled by the value of σ that produces it.

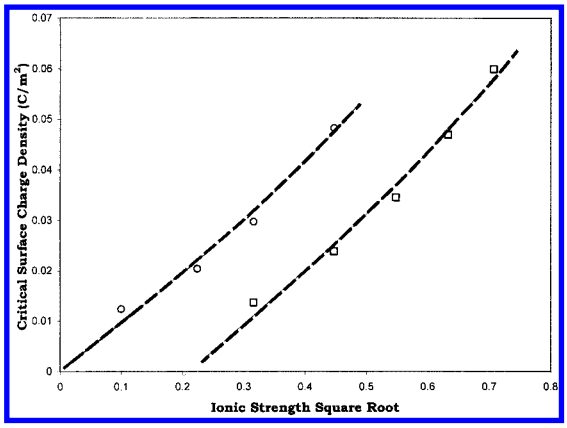

Figure 9. The threshold macroion surface charge density as a function of salt concentration: (○) G1, (□) G3. The points are the values calculated as described in the text. The lines are best fitted through the points.

experimentally to induce binding. In other words, the macroion charges are set equal to Mq_i. We then choose different values of M progressing from unity, thereby incrementally increasing the attractive forces, until the minimum-energy path just touches the particle surface along its entire length and thus represents a bound state.

Theoretical Results

The calculations are performed with specific numerical values for the structural parameters appearing in eqs 12, 13, and 18. The persistence length of the polymer, which determines the Hooke's law constant for bending, was set equal to 25 Å, independent of ionic strength (see discussion below). The distance of closest approach of polymer to macroion a was taken as the mean position of bound polymer segments, inferred experimentally via the approach developed by McQuigg et al.[26] Using the ionic strengths, colloid radii, a, and colloid surface potentials measured at critical conditions for the binding of polyanions to small cationic micelles, McQuigg et al. plotted the Debye−Hückel screened potentials $\psi(r)$ for these spheres and found a common intersection independent of ionic strength. This crossing point (at $r = 6 \pm 0.5$ Å in ref 26) was interpreted as the mean position of bound polyion segments. As shown in Figure 7, screened potential curves for G1 and G3, obtained from the data in Figure 5, also exhibit a crossing point, leading to evaluation of a. For dendrimer G1 of radius 12 Å, $a = 5$ Å; for dendrimer G3 of radius 20 Å, $a = 7.5$ Å. The length L of the binding polymer segment was set to 65 Å, somewhat more than twice a persistence length. This length is sufficient for coverage of a substantial portion of the macroion surface, yet may be short enough for retention of some elastic resilience in the face of chain entropy (it is not much more than a step length in the Kuhn picture of a freely jointed chain).

Figure 8 shows how the polymer segment gradually winds onto the macroion surface as the charge density on the surface increases. There are no abrupt jumps between positions far and near the surface, as was found for winding of DNA onto the histone core of the nucleosome.[24,25] Nevertheless, bound (fully wound) and unbound states, separated by only a small change in the parameter M measuring the macroion charge density are clearly discernible in Figure 8, and a value of M below which the polymer can be considered not bound is readily identified.

Calculated threshold charge densities are plotted as a function of the square root of ionic strength in Figure 9. The points represent the calculated values at ionic strengths identical to those of the experimental measurements. Comparison with the measured values as portrayed in Figure 4 show striking commonality. The measured and calculated threshold surface charge densities required for binding are greater for the smaller dendrimer G1 than for G3 by roughly similar factors. A best-fit line for G1 goes through the origin, as does the extrapolation of the experimental values, and even the slight curvature in the measured data is captured by the calculation. However, as pointed out above, the calculated threshold charge densities are higher than the experimental ones by factors of about 2 to 3.

Discussion

The theoretical model is able to describe some of the features of binding of PDADMAC to the G1 and G3 dendrimers and may therefore have captured the essential reason for a binding threshold: binding can occur only when the charge density of

the macroion is sufficient to overcome the elastic resistance to bending a polymer segment onto the curved macroion surface. This conclusion must be regarded as highly tentative because of the severe simplifications of the model. The replacement of a surface charge density by a linear circumferential density (Figure 6) is very rough. The release of condensed counterions when the polymer binds was not considered (for PDADMAC this limitation may not be severe, because its charge density barely exceeds the threshold for counterion condensation). The size of the polymer binding segment has been, within limits, arbitrarily chosen. The assumption that the length of the binding segment is independent of the macroion radius is only one of convenience, as is the assumption of a polymer persistence length independent of ionic strength. For that matter, the use of a free persistence length as a measure of local bending rigidity in the potential field of the macroion may introduce uncertainties as well.

The question of the dependence of the persistence length of a flexible polymer on ionic strength perhaps deserves some brief commentary. The applicability of current theories to polymers of experimentally typical charge densities and lengths is uncertain.[27] Some of the older experimentally determined trends in persistence length may not have accounted for the supplementary effect of excluded volume. When the excluded volume is properly considered, the persistence length of polystyrene sulfonate is found to increase from 21−39 Å when the ionic strength drops from 0.5 to 0.1 M.[28] For PDADMAC, however, the increase of the apparent persistence length (which includes the effect of excluded volume) in the same range of ionic strengths is only from 25 to 28 Å, and the variation of the actual persistence length can only be less. PDADMAC has a much lower charge density than polystyrene sulfonate, a possible reason for the contrast. In any event, we felt that our best current option for the persistence length of PDADMAC was to take it as independent of salt concentration.

Acknowledgment. This work was supported by NSF Grant DMR 9619772 (P.L.D.) and PHS Grant GM36284 (G.S.M.), as well as NSF Grant DMR 9622609 (G.R.N.).

References and Notes

(1) Margolin, A.; Sheratyuk, S. F.; Izumrudov, V. A.; Zezin, A. B.; Kabanov, V. A. *Eur. J. Biochem.* **1985**, *146*, 625.

(2) Burgess, D. J.; Carless, J. E. *J. Colloid Interface Sci.* **1984**, *98*, 1.

(3) Dubin, P. L.; Gao, J.; Mattison, K. W. *Separation Purification Methods*, **1994**, *23*, 1.

(4) Wiegel, F. W. *J. Phys. A.: Math. Gen.* **1977**, *10*, 299.

(5) Muthukumar, M. *J. Chem. Phys.* **1987**, *86*, 7230.

(6) Evers, O. A.; Fleer, G. J.; Scheutjens, J. M. H. M.; Lyklema, J. *J. Colloid Interface Sci.* **1986**, *111*, 446.

(7) Odijk, T. *Langmuir* **1991**, *7*, 1.

(8) Dubin, P. L.; Chew, C. H.; Gan, L. M. *J. Colloid Interface Sci.* **1989**, *128*, 566.

(9) von Goeler, F.; Muthukumar, M. *J. Chem. Phys.* **1994**, *100*, 7796.

(10) Manning, G. S. *Q. Rev. Biophys.* **1978**, *11*, 179.

(11) Lohman, T. M.; deHaseth, P. L.; Record, M. T., Jr. *Biochemistry* **1980**, *19*, 3522.

(12) (a) Dubin, P. L.; Curran, M. E.; Hua, J. *Langmuir* **1990**, *6*, 707. (b) Dubin, P. L.; Thé, S. S.; McQuigg, D. W.; Gan, L. M. *Langmuir* **1988**, *5*, 89. (c) Mattison, K. W.; Brittain, I. J.; Dubin, P. L. *Biotechnol. Prog.* **1995**, *11*, 632. (d) Yoshida, K.; Morishima, Y.; Mizusaki, M.; Dubin, P. L. *Macromolecules* **1997**, *30*, 6208.

(13) Mattison, K. W.; Dubin, P. L.; Brittain, I. J. *J. Phys. Chem.* **1998**, *103*, 000.

(14) Dubin, P. L.; Chew, C. H.; Gan, L. M. *J. Colloid Interface Sci.* **1989**, *128*, 566.

(15) Wallin, T.; Linse, P. *Langmuir* **1996**, *12*, 305.

(16) (a) Tomalia, D.; Naylor, A. M.; Goddard, W. A., III *Angew. Chem., Int. Ed. Engl.* **1990**, *29*, 138. (b) Newkome, G. R.; Moorefield, C. N.; Vögtle, F. *Dendritic Materials: Concepts, Synthesis, Perspectives*; VCH: Weinheim, Germany, 1996.

(17) Newkome, G. R.; Young, J. K.; Baker, G. R.; Potter, R. L.; Audoly, L.; Cooper, D.; Weis, C. D.; Morris, K.; Johnson, S. J., Jr. *Macromolecules* **1993**, *26*, 2394.

(18) Li, Y.; Dubin, P. L.; Spindler, R.; Tomalia, D. *Macromolecules* **1995**, *28*, 8426.

(19) Zhang, H.; Dubin, P. L.; Spindler, R.; Tomalia, D. *Ber. Bunsen-Ges. Phys. Chem.* **1996**, *100*, 923.

(20) Young, J. K.; Baker, G. R.; Newkome, G. R.; Morris, K. F.; Johnson, C. S., Jr. *Macromolecules* **1994**, *27*, 3464.

(21) Zhang, H.; Dubin, P. L.; Kaplan, J. I.; Moorefield, C. N.; Newkome, G. R. *J. Phys. Chem.* **1997**, *101*, 3494.

(22) Shah, G.; Dubin, P. L.; Kaplan, J. I.; Newkome, G. R.; Moorefield, C. N. *J. Colloid Interface Sci.* **1996**, *182*, 397.

(23) Morawetz, H. Macromolecules in Solution; 2nd ed.; John Wiley & Sons: New York, 1975; p 344−396.

(24) Marky, N.; Manning, G. S. *Biopolymers* **1991**, *31*, 1543.

(25) Marky, N.; Manning, G. S. *J. Mol. Biol.* **1995**, *254*, 50.

(26) McQuigg, D. W.; Kaplan, J. I.; Dubin, P. L. *J. Phys. Chem.* **1992**, *96*, 1973.

(27) Li, H.; Witten, T. A. *Macromolecules* **1995**, *28*, 5921.

(28) Kassapidou, K.; Jesse, W.; Kuil, M. E.; Lapp, A.; Egelhaaf, S.; van der Maarel, J. R. C. *Macromolecules* **1997**, *30*, 2671.